Biochimica et Biophysica Acta 1813 (2011) 1068–1073

Contents lists available at ScienceDirect

Biochimica et Biophysica Acta

journal homepage: www.elsevier.com/locate/bbamcr

Site-directed mutagenesis of the glycine-rich loop of death associated protein kinase (DAPK) identifies it as a key structure for catalytic activity ☆

Laurie K. McNamara [a], Joseph S. Brunzelle [b], James P. Schavocky [a], D. Martin Watterson [a], Valerie Grum-Tokars [a,*]

[a] Department of Molecular Pharmacology and Biological Chemistry, Northwestern University Feinberg School of Medicine, Northwestern University, Chicago, IL 60611, USA
[b] Life Sciences Collaborative Access Team, Advanced Photon Source, Argonne, IL 60439, USA

ARTICLE INFO

Article history:
Received 13 September 2010
Received in revised form 16 November 2010
Accepted 18 November 2010
Available online 29 November 2010

Keywords:
Death associated protein kinase
Calmodulin
Glycine-rich region
Neurodegeneration
Central nervous system
Phosphorylation
Protein kinase inhibitor

ABSTRACT

Death associated protein kinase (DAPK) is a calmodulin (CaM)-regulated protein kinase that is a therapeutic target for central nervous system (CNS) disorders. We report here the results of studies that test the hypothesis of McNamara et al. (2009) that conformational selection in DAPK's glycine-rich region is key for catalytic activity. The hypothesis was tested by site-directed mutagenesis of glutamine-23 (Q23) in the middle of this loop. The glycine-rich loop exhibits localized differences in structure among DAPK conformations that correlate with different stages of the catalytic cycle. Changing the Q23 to a Valine (V23), found at the corresponding position in another CaM regulated protein kinase, results in a reduced catalytic efficiency. High resolution X-ray crystal structures of various conformations of the Q23V mutant DAPK and their superimposition with the corresponding conformations from wild type catalytic domain reveal localized changes in the glycine-rich region. The effect of the mutation on DAPK catalytic activity and the finding of only localized changes in the DAPK structure provide experimental evidence implicating conformational selection in this domain with activity. This article is part of a Special Issue entitled: 11th European Symposium on Calcium.

1. Introduction

Protein kinases are macromolecular catalysts that serve critical intracellular signal transduction roles in eukaryotic cells. The rate-limiting step in the catalytic cycle of a signaling protein kinase is the release of the products, ADP and the phosphorylated protein product. There is a rapidly increasing knowledge over the past few years about the comparative differences in structures of kinases representative of the various catalytic cycle stages. This includes comparative changes among kinases complexed with ADP, a reaction product, and non-hydrolysable analogs of ATP, a reaction substrate. The high resolution structures of different conformational states of various kinases have provided insight into how kinase structure might be related to the stage of the catalytic cycle. In this regard, we recently [1] determined and analyzed the structures of various conformations of the calmodulin (CaM) regulated protein kinase, death associated protein kinase (DAPK), in attempts to gain insight into how this particular kinase's structure is altered with various states containing bound substrate analog or reaction product as well as the apoenzyme. Superimposition revealed localized changes in the glycine-rich region, sometimes called the P-loop, that correlated with more open or closed conformations of the glycine-rich region centered around glutamine-23 (Q23).

The emergent hypothesis from the work of McNamara et al. [1] was that the portion of the glycine-rich region around Q23 may be essential for interaction with ATP and ADP, making it important in catalytic activity. This report directly addresses this hypothesis through the use of site-directed mutagenesis of Q23 to a valine (V23) found in another CaM regulated protein kinase, analysis of the activity of the mutant kinase, and comparison of the differences in selected conformational states of the mutant kinase. These results are consistent with the hypothesis of McNamara et al. [1]. Further, the analyses raise the possibility that targeting the conformation of this particular region of DAPK may prove fruitful for the identification of novel inhibitors that could work indirectly by modulating the conformational state of DAPK in this region.

The interest in DAPK as a central nervous system (CNS) drug discovery target is based on the in vivo role of DAPK in animal model disease progression that is dependent on the kinase domain's catalytic activity [2–6]. Bioavailable DAPK inhibitors administered during clinically relevant therapeutic time windows attenuate synaptic dysfunction and improve longer term neurological outcomes. More recent clinical data [7] has mapped an age-onset AD susceptibility locus to the DAPK gene. Therefore, there is an increasing body of evidence that links the DAPK catalytic activity to disease progression and its attenuation via use of bioavailable small molecule inhibitors of activity. The interest in DAPK catalytic domain activity from a potential CNS

☆ This article is part of a Special Issue entitled: 11th European Symposium on Calcium.

* Corresponding author.
E-mail address: v-tokars@northwestern.edu (V. Grum-Tokars).

0167-4889/$ – see front matter © 2010 Elsevier B.V. All rights reserved.
doi:10.1016/j.bbamcr.2010.11.011

disease intervention perspective adds a translational emphasis to the testing of the hypothesis of McNamara et al. [1] about the glycine-rich region.

2. Materials and methods

2.1. Generation of DAPKQ23V mutant

The DAPKQ23V mutant was created in the pASK-IBA-3 expression vector (Sigma-GenoSys) using the Quik Change Site-Directed Mutagenesis Kit (Stratagene). The mutagenesis procedures and construct has been previously described in Velentza et al. [8]. The mutation was confirmed by DNA sequence analysis using the vector specific primer 5'-GAGTTATTTTACCACTCCCT-3' and an ABI 3730 DNA Sequencer with Big Dye v.3.1. The plasmids were transformed into XL1-Blue *Escherichia coli*.

2.2. Protein production of DAPK and DAPKQ23V

The constitutively active catalytic domain consisting of amino acids 1–285 of DAPK and DAPKQ23V were expressed and purified as previously described [8]. For crystallization trials of enzyme in complex with Mg^{2+} and ADP or AMPPNP, the anion exchange chromatographic step, which included the use of EDTA [8], was eliminated from the purification protocol. As described in McNamara et al. [1], the cells were sonicated in a buffer consisting of 100 mM Tris–HCl, pH 8.0, 0.25 M NaCl, 0.7 mg/L pepstatin A, 0.01% Triton X-100, and 1 mM DTT. After concentration, the buffer for the protein was exchanged into 20 mM Tris–HCl pH 8.0 and 0.25 M NaCl.

2.3. Activity assays

Enzyme assays and kinetic analyses were done as previously described [8]. Briefly, concentrations of the peptide substrate from 2.5 μM–50 μM were incubated with 200 μM ATP and [γ-^{32}P]-ATP (2.5 μCi per reaction) in assay buffer (50 mM Hepes, pH 7.5, 1 mM DTT, 5 mM $MgCl_2$, 150 mM KCl, 15 mM NaCl) for 12 min at 25 °C either with or without the DAPK catalytic domain. Peptide 38 (KKRPQRRYSNVF) from the DAPK peptide substrate discovery studies was used for the kinetics determination [8]. Reactions were initiated by the addition of the DAPK catalytic domain. Reaction mixture aliquots were spotted onto P-81 paper (Whatman, Clifton, NJ), washed with 75 mM H_3PO_4 and 95% ethanol, and quantified by scintillation counting in EcoScint O (National Diagnostics, Atlanta, GA). Less than 10% of the peptide was consumed under these conditions. Kinetic data were analyzed by nonlinear regression curve fitting, using the Michaelis–Menten equation (Prism version 4.0, GraphPad Software, Inc.). Catalytic efficiency was calculated as the k_{cat}/K_m. For ATP kinetics, the same procedure was used except the peptide concentration was held constant at 5× the K_m of the peptide substrate with varying concentrations of ATP from 1 μM–25 μM.

2.4. Crystallization, data collection, and structure determination

For the complexes of DAPKQ23V with nucleotides, a protein solution at 5.5 mg/mL in 20 mM Tris pH 8.0, 1 mM DTT, 1 mM EDTA, 0.25 M NaCl was incubated with 1 mM of either AMPPNP or ADP at 4 °C. Incubation times of nucleotide and protein varied from 30 min to 24 h. Crystallization conditions were determined using the 96-well plate NeXtal AmSO4 suite screen (Qiagen, Valencia, CA) using the sitting drop method for crystallization. Crystallization plates were incubated at 295 K and crystals appeared within 15 h. Crystals were harvested directly from the 96-well plate and were flash frozen in cryoprotection solvent that consisted of the mother liquor supplemented with 30% sucrose and 3.8 mM of either ADP or AMPPNP. Structures which contained Mg^{2+} were also preincubated with 10 mM $MgCl_2$ and the cryoprotection solution contained 50 mM $MgCl_2$.

Data sets were integrated and merged using HKL2000 [9]. Structures were determined by molecular replacement using MolRep [10] using the original DAPK model [11] (PDB ID: 1JKS) with waters removed. Interactive rounds of model building with Coot [12], refinement with Refmac5 [13], and solvent addition with ARP/wARP [14] led to the final refined model. Superpositions of protein structures were done using Least Squares Fitting (LSQ) within Coot using all atoms. Figures were prepared with Pymol [15]. The coordinates of DAPKQ23V-AMPPNP, DAPKQ23V-ADP, DAPKQ23V-AMPPNP-Mg^{2+}, DAPKQ23V-ADP-Mg^{2+}, DAPKQ23K, and DAPKQ23K-AMPPNP have been deposited in the PDB (3GU4, 3GU6, 3GU5, 3GU7, 3DGK, and 3DFC, respectively).

3. Results

3.1. Rationale and design

DAPK is a member of the calmodulin regulated protein kinases (CaMKs), intracellular enzymes whose activity is modulated by intracellular calcium signaling via their respective calmodulin (CaM) regulatory subunits. Of the greater than 30 CaMKs known, DAPK and two other CaM regulated protein kinases, myosin light chain kinase (MLCK), and phosphorylase kinase (PhosK), are especially interesting due their restrictive substrate preferences compared to other CaMKs that are more promiscuous in their phosphorylation of numerous and diverse protein substrates [16]. A sequence alignment of the kinase domain from human DAPK, MLCK and PhosK is presented in Fig. 1a and highlights common features of the enzymes. This information has been mapped onto a three-dimensional representation of the conserved core of the catalytic domain (PDB ID: 3F5G), represented in Fig. 1b. The domain arrangement consists of a smaller N-terminal domain that is predominantly β-sheet, and a larger C-terminal domain containing mostly α-helices, which are connected by a hinge region. A glycine-rich region involved in hydrogen bonding to nucleotide phosphates of ATP [1] contains residues found in close proximity to the proposed peptide substrate recognition regions of protein kinases [8].

Previous studies on DAPK raised the possibility that the glycine-rich loop region might be key for catalytic activity and identified the region around Q23 as especially attractive [1]. We directly tested this possibility by introducing a site-directed mutant at this position. This residue corresponds to a valine and a lysine in PhosK and MLCK, respectively. By mutating this position to a closely related kinase, we sought to elicit a localized change in the loop region without perturbing the overall structure. We chose to begin with a Q23V mutation, corresponding to the residue of PhosK. Like DAPK, PhosK lacks the third conserved glycine found in 85% of known kinases [17]. The mutation of Q23 to Val resulted in a DAPK glycine-rich loop sequence -Leu-Gly-Ser-Gly-Val23-Phe-Ala-Val-Val.

3.2. The mutation of glutamine 23 to valine results in a loss of DAPK catalytic efficiency

The effect of the Q23K point mutation on DAPK catalytic activity is summarized in Table 1. The mutation resulted in an increase in the K_m for the peptide substrate from 6.8 μM to 14.2 μM, while the K_m value for ATP remained the same. The k_{cat} value determined for both substrates is reduced by more than 10-fold in DAPKQ23V compared to the wild type DAPK. The overall catalytic efficiency (k_{cat}/K_m) for the enzyme is reduced from 12.2 $\mu M^{-1}\,min^{-1}$ to 0.5 $\mu M^{-1}\,min^{-1}$, due primarily to changes in k_{cat}.

3.3. The crystal structures of DAPKQ23V-AMPPNP and DAPKQ23V-AMPPNP-Mg^{2+} and their comparison to wild type complexes

The three-dimensional structures of DAPKQ23V in complex with AMPPNP and AMPPNP-Mg^{2+} were determined by X-ray crystallography to resolutions of 1.35 and 1.65 Å, respectively. Data collection

a

```
huDAPk.pro  TVFRQENVDDYYDT---GEELGSGQFAVVKKCREKSTGLQYAAKFIK-----KRRTKSSRRGVSREDIEREVSILKEIQ-  71
huMLCK.pro  TINTEQKVSDFYDI---EERLGSGKFGQVFRLVEKKTRKVWAGKFFK-----AYSAKE------KENIRQEISIMNCLH-  65
huPHKG1.pro P--DSHSAQDFYENYEPKEILGRGVSSVVRRCIHKPTSQEYAVKVIDVTGGGSFSPEEVRE--LREATLKEVDILRKVSG  76

huDAPk.pro  HPNVITLHEVYENKTDVILILELVAGGELFDFLAEKE-SLTEEEATEFLKQILNGVYYLHSLQIAHFDLKPENIMLLDRN 150
huMLCK.pro  HPKLVQCVDAFEEKANIVMVLEIVSGGELFERIIDEDFELTERECIKYMRQISEGVEYIHKQGIVHLDLKPENIMCVNKT 145
huPHKG1.pro HPNIIQLKDTYETNTFFFLVFDLMKRGELFDYLTEK-VTLSEKETRKIMRALLEVICTLHKLNIVHRDLKPENILLDDNM 155

huDAPk.pro  VPKPRIKIIDFGLAHKIDFGNEFKNIFGTPEFVAPEIVNY----EPLGL--EADMWSIGVITYILLSGASPFLGDTKQET 224
huMLCK.pro  GT--RIKLIDFGLARRLENAGSLKVLFGTPEFVAPEVINY----EPIGY--ATDMWSIGVICYILVSGLSPFMGDNDNET 217
huPHKG1.pro ----NIKLTDFGFSCQLEPGERLREVCGTPSYLAPEIIECSMNEDHPGYGKEVDMWSTGVIMYTLLAGSPPFWHRKQMLM 231

huDAPk.pro  LANVSAVNYEFEDEYFSNTSALAKDFIRRLLVKDPKKRMTIQDSLQHPWIKPKDTQQALS                    284
huMLCK.pro  LANVTSATWDFDDEAFDEISDDAKDFISNLLKKDMKNRLDCTQCLQHPWLM-KDTKNMEA                    276
huPHKG1.pro LRMIMSGNYQFGSPEWDDYSDTVKDLVSRFLVVQPQNRYTAEEALAHPFFQQYLVEEVRH                    291
```

b

Fig. 1. a) Sequence alignment of DAPK, MLCK, and PhosK (NCBI sequences NP_004929, NP_444253, NP_006204). The glycine-rich loop region, catalytic lysine and start of the activation domain (DRG) are highlighted b) Three dimensional representation of DAPK in the presence of ADP (PDB ID: 3F5G). The glycine-rich region is colored tan, the catalytic lysine in red and DRG in green.

and refinement statistics are shown in Table 2. Fourier difference ($F_o - F_c$) omit maps (not shown) contoured at the 3.0σ level revealed electron density for the nucleotides at the expected location, between the N- and C-terminal domains. The occupancy for the γ-phosphate of AMPPNP in the DAPKQ23V-AMPPNP-Mg^{2+} and DAPKQ23V-AMPPNP structures were adjusted to 0.25 and 0.5 to eliminate negative density. As was the case for the wild type structure of DAPK-AMPPNP-Mg^{2+} (PDB ID: 3F5U), one Mg^{2+} ion is seen in the Q23V-AMPPNP-Mg^{2+} structure. The Mg^{2+} ion is coordinated by six ligands, which include the OD2 Asp 161 (2.1 Å), the OD1 Asn144 (2.6 Å), an HOH (1.6 Å), the O1A of the α-phosphate (2.1 Å), an HOH (2.1 Å), and the O3G of the γ-phosphate (2.4 Å). In the DAPK-AMPPNP-Mg^{2+} structure, the Mg^{2+} is coordinated to the O2G of the γ-phosphate rather than the OD1 of Asn144.

In contrast to the DAPK-AMPPNP-Mg^{2+} structure, where Q23 and the adjacent Phenylalanine 24 (F24) appear to have two conformations each, Valine 23 (V23) in the DAPKQ23V-AMPPNP-Mg^{2+} structure can be modeled into a single conformation with F24 in the "up" conformation. In the absence of Mg^{2+}, the DAPKQ23V-AMPNP is modeled with a single conformation of F24 in the "up" position and two conformations for V23. A superposition of the DAPKQ23V-AMPPNP and DAPKQ23V-AMPPNP-Mg^{2+} structures shows that the loop region around residue 23 is more closed in the DAPKQ23V-AMPPNP structure when the second conformation of V23 is considered.

Table 1
Kinetics for DAPK and DAPKQ23V. Assay conditions are described in Section 2.3.

Protein	DAPK	DAPKQ23V
Km (μM) peptide	6.8 ± 0.5	14.2 ± 1.0
kcat (min^{-1}) Peptide	83.3 ± 2.4	7.4 ± 0.4
kcat/Km ($\mu M^{-1} min^{-1}$) Peptide	12.2	0.5
Km (μM) ATP	4.1 ± 0.4	4.4 ± 0.4
kcat (min^{-1}) ATP	83.9 ± 3.9	7.0 + 0.3
kcat/Km ($\mu M^{-1} min^{-1}$) ATP	20.6	1.6

3.4. The crystal structures of DAPKQ23V-ADP and DAPKQ23V-ADP-Mg^{2+} and their comparison to wild type complexes

In addition to the AMPPNP structures, DAPKQ23V was solved in complex with ADP and ADP-Mg^{2+} at 1.50 Å and 1.90 Å, respectively. Data collection and refinement statistics are shown in Table 2. Electron density for the ADP was clearly visible in the mutant structures in the presence and absence of Mg^{2+}. One Mg^{2+} ion was modeled in the structure with an octahedral coordination including the OD2 of Asp161 (2.2 Å), an HOH (2.5 Å), the O3B of ADP (2.3 Å), an HOH (2.5 Å), an HOH (1.7 Å), and the O1A ADP (2.2 Å). This differs

Table 2
Crystallographic data collection and refinement statistics for the DAPKQ23V-AMPPNP, DAPKQ23V-AMPPNP-Mg^{2+}, DAPKQ23V-ADP and DAPKQ23V-ADP-Mg^{2+} structures. All structures have been deposited in the protein data bank.

	DAPKQ23V-AMPPNP	DAPKQ23V-AMPPNP-Mg^{2+}	DAPKQ23V-ADP	DAPKQ23V-ADP-Mg^{2+}
Ligand	AMPPNP	AMPPNP-Mg^{2+}	ADP	ADP-Mg^{2+}
PDB code	3GU4	3GU5	3GU6	3GU7
Space group		P212121		
Unit-cell parameter (Å)	$a=46.9$	$a=46.9$	$a=46.9$	$a=46.89$
	$b=62.4$	$b=62.5$	$b=62.3$	$b=62.4$
	$c=88.4$	$c=88.6$	$c=88.1$	$c=88.3$
X-ray source	LSCAT-21-ID-F	LSCAT-21-ID-G	LSCAT-21-ID-G	LSCAT-21-ID-G
Wavelength (Å)	0.97872	0.97857	0.97857	0.97857
Resolution (Å)	30.0–1.35(1.40–1.35)	30.0–1.65(1.71–1.65)	30.0–1.50(1.55–1.50)	30.0–1.90(1.97–1.90)
No. of unique reflections	57,021	32,180	42,344	21,031
Completeness	98.84(97.33)	99.83(98.11)	99.44(94.30)	99.91(99.48)
Redundancy	5.7(5.6)	7.0(7.0)	7.3(6.9)	6.8(6.9)
Mean I/σ(*I*)	12.7(3.3)	13.1(4.7)	11.5(3.8)	10.5(4.7)
*R*merge	0.059(0.354)	0.070(0.409)	0.079(0.487)	0.079(0.412)
Final *R*work	0.184(0.207)	0.175(0.204)	0.183(0.218)	0.170(0.185)
Final *Rfree*	0.211(0.235)	0.219(0.281)	0.213(0.240)	0.228(0.280)
Bond lengths (Å)	0.008	0.012	0.009	0.015
Bond angles ( )	1.31	1.47	1.31	1.68
Average B-factors (Å)	17.54	20.92	17.9	22.6
Main chain	14.59	18.50	15.61	20.27
Side chain + Solvent	19.77	22.81	19.73	24.56
Ligand	20.10	19.15	28.90	30.95

from DAPK-ADP-Mg^{2+} (PDB ID: 3F5G), which shows coordination to OE2 of Glu14 and OD1 of Asn144, rather than waters. There is an alternative conformation for the β-phosphate in the absence of Mg^{2+}.

The residues at V23 and F24 were modeled in two conformations for the DAPKQ23V-ADP-Mg^{2+} and DAPKQ23V-ADP structures. This is similar to the loop regions of the corresponding wild type ADP complexes DAPK-ADP-Mg^{2+} and DAPK-ADP (PDB ID: 3F5G and 3EH9, respectively). The structures of DAPKQ23V-ADP-Mg^{2+} and DAPK-ADP-Mg^{2+} were superimposed as well on the DAPKQ23V-ADP and DAPK-ADP structures. Differences were noted in the glycine-rich region for the overlay of DAPKQ23V-ADP with DAPK-ADP, with an r.m.s. deviation of 2.56 Å for the Cα atoms of residues 20–25. The r.m.s deviation value for this region of DAPKQ23V-ADP-Mg^{2+} and DAPK-ADP-Mg^{2+} is 0.83 Å. The superpositions suggest that the mutant DAPK in complex with ADP has a glycine-rich loop that is more closed compared to the corresponding wild type structures. The loop closure, however, is more evident when the non-Mg^{2+} structures are compared.

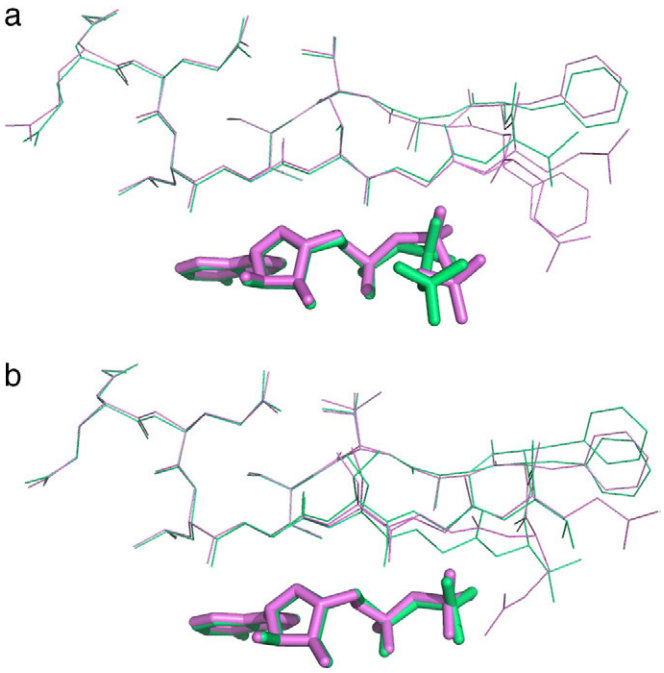

Fig. 2. (a) Ligand binding site of DAPK-AMPPNP-Mg^{2+} (magenta) and DAPKQ23V-AMPPNP-Mg^{2+} (green). Included is a superposition of the glycine-rich loop residues 17–27. (b) Ligand binding site of DAPK-ADP-Mg^{2+} (magenta) and DAPKQ23V-ADP-Mg^{2+} (green). Included is a superposition of the glycine-rich loop residues 17–27. Alternate conformations are shown in these traces.

3.5. Comparing members of the catalytic cycle

Fig. 2a shows a superposition of DAPK-AMPPNP-Mg^{2+} and Q23V-AMPPNP-Mg^{2+}. The DAPK-AMPPNP-Mg^{2+} complex is shown in magenta and has two conformations present for residues Q23 and F24. The Q23V mutant shown in green maintains a single conformation in the crystal structure. The closed conformation for the wild type

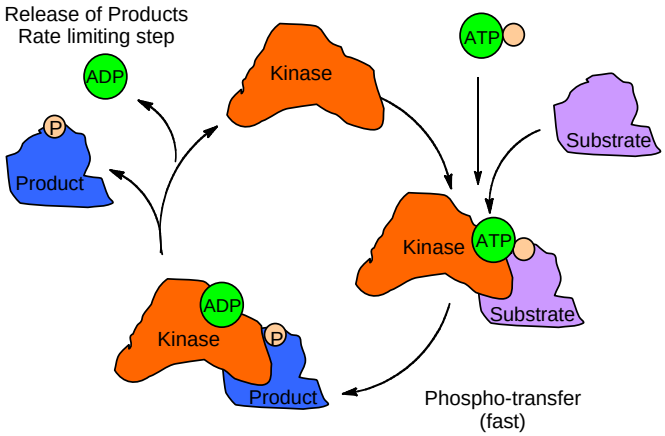

Fig. 3. Kinetic scheme for phosphoryl transfer reaction. The kinase binds two substrates, ATP and a peptide or protein substrate. Once substrate is bound, the phosphoryl transfer step proceeds rapidly relative to product release.

enzyme involves a repositioning of the glycine-rich loop that is not evident with the Q23V mutant. The bottom panel is a superposition of DAPK-ADP-Mg^{2+} and DAPK-Q23V-ADP- Mg^{2+}. The DAPK-ADP-Mg^{2+} complex shown in magenta displays two conformations for Q23. The Q23V-ADP- Mg^{2+} complex has the valine in two orientations as well as F24. In the crystal structures, the R-group of the Q23V appears to be pointed away from ADP when Mg^{2+} is present.

4. Discussion

The studies reported here provide a more direct link between conformations of the glycine-rich region of DAPK and enzyme activity. As schematically illustrated in Fig. 3, the various conformations of DAPK with bound substrate or product can be considered reflective of transient states in a catalytic cycle. The protein kinase binds the two substrates, ATP and protein, and facilitates a phosphoryl transfer reaction, followed by release of products. The phosphoryl transfer step is fast, while the release of products is the rate-limiting step [18]. The demonstration that a point mutation in the glycine-rich region can result in only localized changes in structure yet diminish catalytic efficiency significantly is consistent with the hypothesis that this loop is a critical modulator of DAPK catalytic activity. As a logical extension of the results presented here, we also explored the potential impact of a Q23K mutation corresponding to the closely related MLCK region. This point mutation was also detrimental to catalytic activity due mainly to the k_{cat} term (data not shown) and also resulted in only localized conformational differences (see PDB IDs: 3DFC, 3DGK). Superimposition of DAPK-AMPPNP (magenta), DAPKQ23V-AMPPNP (grey), and DAPKQ23K-AMPPNP (cyan) reveal (Fig. 4) a common trend of a more closed state for the glycine-rich loop in the mutants, and altered geometry of the nucleotide at the γ-phosphate.

Clearly, the glycine-rich loop region around Q23 plays an important role in catalysis, but the manner in which this particular residue contributes to alteration of loop conformation is not as evident. Results from examination of this corresponding region in other Ser/Thr protein kinases are consistent with those reported here. For example, mutagenesis of Ser53 in cAMP-dependent protein kinase (PKA), corresponding to Q23 of DAPK, resulted in a loss of kinase activity [19]. Similarly, PhosK, exhibits a loss of activity when V29, corresponding to Q23, is mutated to a serine [20]. The PhosK-V29S mutant had an apparent increase in affinity for ADP. It was suggested [20] that the apparent increase in affinity was due to an altered conformation leading to binding of the nucleotide product with greater affinity. Our kinetic and structural results for DAPK Q23 mutant are consistent with such models.

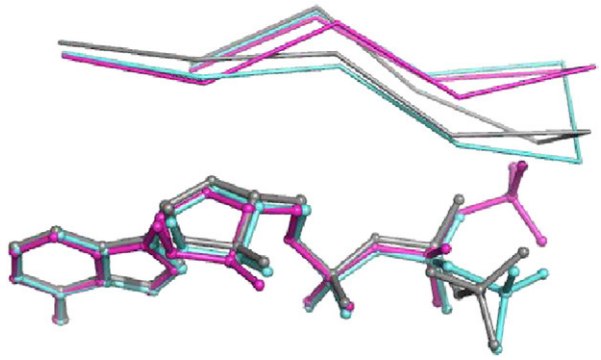

Fig. 4. Superposition of the glycine-rich region of DAPK, DAPKQ23V and DAPKQ23K in complex with AMPPNP. Residues 19–27 are depicted as a carbon backbone trace and AMPPNP is rendered as a ball and stick model. Wild type DAPK in magenta, DAPKQ23V in cyan and DAPKQ23K in gray. An alternative conformation is observed for the AMPPNP γ-phosphate of the Q23 mutants relative to the wild type.

The hypothesis derived from the work of McNamara et al. [1] was that the portion of the glycine-rich region around Q23 may be essential for interaction with ATP and ADP, making it important in catalytic activity. The current data presented for the DAPKQ23V mutant support this hypothesis. A logical extension of the hypothesis based on the data presented here is that conformational selection around the glycine-rich region of DAPK might be a potential mechanism for modulating kinase activity. For example, restricting conformational sampling by this region of DAPK could result in restriction of phosphate transfer or generation of a more closed conformation. Mechanistically, the latter could result in a decreased release of product, whereas the former could derive from the inability of the Q23 side chain to orient and stabilize the ligand or from an alteration of the geometry around the phosphates such that a less than ideal arrangement would be provided for the phosphoryl transfer.

5. Conclusions

The structures reported here are the first DAPK mutant structures and the first for any kinase altered in the glycine-rich region. Structural changes brought about by targeted point mutations are localized to the loop region that contains the mutation and result in significant changes in catalytic efficiency.

Acknowledgements

This work was supported in part by NIH awards NS056051 and AG031311 (DMW).

References

[1] L.K. McNamara, D.M. Watterson, J.S. Brunzelle, Structural insight into nucleotide recognition by human death-associated protein kinase, Acta Crystallogr. D Biol. Crystallogr. 65 (2009) 241–248.
[2] J.M. Craft, D.M. Watterson, S.A. Frautschy, L.J. Van Eldik, Aminopyridazines inhibit beta-amyloid-induced glial activation and neuronal damage in vivo, Neurobiol. Aging 25 (2004) 1283–1292.
[3] A.M. Schumacher, A.V. Velentza, D.M. Watterson, Death-associated protein kinase as a potential therapeutic target, Expert Opin. Ther. Targets 6 (2002) 497–506.
[4] A.M. Schumacher, A.V. Velentza, D.M. Watterson, M.S. Wainwright, DAPK catalytic activity in the hippocampus increases during the recovery phase in an animal model of brain hypoxic-ischemic injury, Biochim. Biophys. Acta 1600 (2002) 128–137.
[5] M. Shamloo, L. Soriano, T. Wieloch, K. Nikolich, R. Urfer, D. Oksenberg, Death-associated protein kinase is activated by dephosphorylation in response to cerebral ischemia, J. Biol. Chem. 280 (2005) 42290–42299.
[6] A.V. Velentza, M.S. Wainwright, M. Zasadzki, S. Mirzoeva, A.M. Schumacher, J. Haiech, P.J. Focia, M. Egli, D.M. Watterson, An aminopyridazine-based inhibitor of a pro-apoptotic protein kinase attenuates hypoxia-ischemia induced acute brain injury, Bioorg. Med. Chem. Lett. 13 (2003) 3465–3470.
[7] Y. Li, A. Grupe, C. Rowland, P. Nowotny, J.S. Kauwe, S. Smemo, A. Hinrichs, K. Tacey, T.A. Toombs, S. Kwok, J. Catanese, T.J. White, T.J. Maxwell, P. Hollingworth, R. Abraham, D.C. Rubinsztein, C. Brayne, F. Wavrant-De Vrieze, J. Hardy, M. O'Donovan, S. Lovestone, J.C. Morris, L.J. Thal, M. Owen, J. Williams, A. Goate, DAPK1 variants are associated with Alzheimer's disease and allele-specific expression, Hum. Mol. Genet. 15 (2006) 2560–2568.
[8] A.V. Velentza, A.M. Schumacher, C. Weiss, M. Egli, D.M. Watterson, A protein kinase associated with apoptosis and tumor suppression: structure, activity, and discovery of peptide substrates, J. Biol. Chem. 276 (2001) 38956–38965.
[9] Z. Otwinowski, W. Minor, Processing of X-ray diffraction data collected in oscillation mode, Macromol. Crystallogr. Pt A 276 (1997) 307–326.
[10] A. Vagin, A. Teplyakov, MOLREP: an automated program for molecular replacement, J. Appl. Crystallogr. 30 (1997) 1022–1025.
[11] V. Tereshko, M. Teplova, J. Brunzelle, D.M. Watterson, M. Egli, Crystal structures of the catalytic domain of human protein kinase associated with apoptosis and tumor suppression, Nat. Struct. Biol. 8 (2001) 899–907.
[12] P. Emsley, K. Cowtan, Coot: model-building tools for molecular graphics, Acta Crystallogr. D60 (2004) 2126–2132.
[13] G.N. Murshudov, A.A. Vagin, E.J. Dodson, Refinement of macromolecular structures by the maximum-likelihood method, Acta Crystallogr. D Biol. Crystallogr. 53 (1997) 240–255.
[14] A. Perrakis, T.K. Sixma, K.S. Wilson, V.S. Lamzin, wARP: Improvement and extension of crystallographic phases by weighted averaging of multiple-refined dummy atomic models, Acta Crystallogr. D Biol. Crystallogr. 53 (1997) 448–455.
[15] W.L. DeLano, The PyMol Molecular Graphics System, DeLano Scientific, San Carlos, CA, 2002.

[16] T.J. Lukas, S. Mirzoeva, D.M. Watterson, Calmodulin-regulated protein kinases, in: L.J. Van Eldik, D.M. Watterson (Eds.), Calmodulin and Signal Transduction, Academic Press, New York, 1998, pp. 65–168.
[17] W. Hemmer, M. McGlone, I. Tsigelny, S.S. Taylor, Role of the glycine triad in the ATP-binding site of cAMP-dependent protein kinase, J. Biol. Chem. 272 (1997) 16946–16954.
[18] J.A. Adams, Kinetic and catalytic mechanisms of protein kinases, Chem. Rev. 101 (2001) 2271–2290.
[19] R.T. Aimes, W. Hemmer, S.S. Taylor, Serine-53 at the tip of the glycine-rich loop of cAMP-dependent protein kinase: role in catalysis, P-site specificity, and interaction with inhibitors, Biochemistry 39 (2000) 8325–8332.
[20] J.H. Lee, S. Maeda, K.L. Angelos, S.G. Kamita, C. Ramachandran, D.A. Walsh, Analysis by mutagenesis of the ATP binding site of the gamma subunit of skeletal muscle phosphorylase kinase expressed using a baculovirus system, Biochemistry 31 (1992) 10616–10625.